Materials Advances

ROYAL SOCIETY OF CHEMISTRY

PAPER

View Article Online
View Journal

Cite this: DOI: 10.1039/d5ma01533b

Fabrication of multifunctional poly(acrylic acid) hydrogels using a nickel–carboxymethyl cellulose crosslinker

Md. Sohanur Rahman,[a] Maisha Rahman,[a] Md. Mahamudul Hasan Rumon,[ab] Chanchal Kumar Roy[a] and Md. Mahbub Alam *[a]

Received 31st December 2025,
Accepted 7th March 2026

DOI: 10.1039/d5ma01533b

rsc.li/materials-advances

The derivatives of cellulose, particularly carboxymethyl cellulose (CMC), are among the popular physical crosslinkers used to improve the mechanical toughness and self-healing capability of polymeric hydrogels. In this work, we developed a multifunctional polyacrylic acid (PAA) hydrogel reinforced with CMC and nickel nanoparticles (Ni-NPs), creating a nanocomposite that combines mechanical robustness, dynamic self-repair, moderate electrical conductivity and magnetic properties. The successful incorporation of Ni-NPs in the hydrogel network was confirmed using FTIR spectra and FESEM images. TGA and DTGA studies revealed that the thermal stability of CMC was significantly improved upon the incorporation of Ni-NPs. By varying the nanoparticle content, we observed a tunable balance between mechanical strength and stretchability, with higher amounts of Ni-NPs yielding markedly enhanced tensile performance. It was found that as the amount of Ni-NPs increased, the tensile strength increased, while the elongation at the break of the hydrogel decreased. The presence of Ni-NPs also introduced reversible ionic and coordination interactions that promoted efficient self-healing. Additionally, the nanocomposite exhibited notable electrical conductivity and responsiveness to magnetic stimuli, expanding its potential functionality. All these features highlight the potential of PAA–Ni–CMC hydrogels in biomedical and soft-device applications, such as flexible sensors, tissue-interfacing materials, and magnetically controlled drug-delivery platforms, where mechanical strength, self-healing, and moderate conductivity are desirable.

1. Introduction

Hydrogels are well-known smart materials that have a variety of applications, such as in tissue engineering,[1] drug delivery,[2] sensing technology,[3] biochemical applications,[4] biochemical separation,[5] and catalytic reactions,[6] due to their 'soft and wet' nature and unique combination of stimulus responsiveness and biocompatibility.[7] Hydrogel materials have drawn significant research interest in recent years because of their high sensitivity to the changes in stimuli such as light,[8] temperature,[9] pressure,[10] solvents,[11] pH,[12] electric field,[13] and magnetic field.[14] The preparation, modification, and development of hydrogels have recently seen some fantastic accomplishments. However, it is exceedingly difficult for hydrogels to be effective in biomedical engineering applications because hydrogels with poor toughness are typically accompanied by very limited stretchability.

The inclusion of cross-linkers in the hydrogel network has a significant impact on the mechanical properties of hydrogels.[15] Most of the conventional chemical cross-linkers form covalent bonds with polymer chains, which improve the toughness and Young's modulus but compromise the stretchability.[16] Recent studies show that the inclusion of physical cross-linking may lead to high toughness and flexibility.[17] Physical cross-linking provides weak frictional resistance during polymer chain movement and ensures continuous energy dissipation during deformation, which provides viscoelastic properties to the hydrogel.[18] Physical cross-linking in the polymeric hydrogel network can be introduced through ionic interactions,[19] hydrogen bonds,[20] and host–guest interactions.[21] In hydrogels, polymeric dispersive interactions of the nanomaterial surface provide an alternative to traditional physical cross-linking.[22] Although remarkable improvement in the mechanical behavior of hydrogels have been achieved through the development of nanocomposites incorporating nanoclay,[23] carbon nanotubes,[24] silica nanoparticles,[25] metal nanoparticles,[26] *etc.*, their mechanical performance still falls short of the desired levels, limiting their practical applications. The major drawbacks include random bonding of the polymer and cross-linker, which incurs non-uniform stress distribution.[22]

On the other hand, electrically conductive hydrogels are promising materials that can be used as both implantable[27,28]

[a] *Department of Chemistry, Bangladesh University of Engineering and Technology, Dhaka, Bangladesh. E-mail: mdmahbub@chem.buet.ac.bd*
[b] *Department of Chemistry, Indiana University, Bloomington, USA*

and wearable[29,30] bioelectronics devices due to the ability of the hydrogel materials to mimic the features of biological tissues, and their electrical conductivity. These conductive hydrogels possess all the properties of conventional hydrogels, such as tunable mechanical properties, flexibility, swelling capacity, hydrophilicity, and the capacity to conduct electricity. Electrical conductivity can be introduced in a hydrogel network either by using conducting polymers[31–33] or by incorporating carbon nanotubes,[34] metal nanowires[35] or nanoparticles[36,37] in the hydrogel.

Hydrogels combined with nanoparticles result in novel superstructures, which have gained significant attention from researchers in the last few years.[38–40] The combination of the two completely different types of materials provides structural diversity in the composite structure and is thought to generate multiformity in properties. Moreover, the components of these superstructures are easy to tune depending on the target applications and, therefore, provide a wide range of tunability and multifunctionality. Therefore, hydrogel-nanoparticle composites possess immense potential for numerous applications, particularly in the areas of diagnosis, prevention, and treatment of human diseases.[41–43] In addition to electrical conductivity, responsiveness to a magnetic field is another important property of hydrogel composite materials. Hydrogels with magnetic properties, usually known as ferrogels, can be obtained by incorporating magnetic particles in the hydrogel matrices.[44] It is no surprise that the sensitivity to the external magnetic field strongly depends on the volume fraction of the magnetic nanoparticles in the hydrogel matrices, as found by Liu *et al.*[45] Hydrogels with magnetic sensitivity have been broadly used, particularly in biological fields such as magnetic resonance imaging[46] and targeted drug delivery.[47,48]

In this study, we have introduced a metal-incorporated cellulose-based crosslinker to improve the mechanical strength and to impart electrical conductivity and magnetic sensitivity to conventional polyacrylic acid (PAA) hydrogel matrices. We have also prepared PAA–Ni hydrogels and PAA–CMC hydrogels to compare the properties of the PAA–Ni–CMC nanocomposite. The mechanical properties, self-healing capability, electrical conductivity, magnetic sensitivity, and swelling behaviour of these hydrogels have been investigated for various compositions of the crosslinker.

2. Experimental

2.1. Chemicals and materials

Nickel chloride hexahydrate, acrylic acid (AA), and *N*,*N*′-methylene bis-acrylamide (MBA) were purchased from Sigma Aldrich Chemical Co. Hydrazine hydrate, sodium hydroxide, sodium carboxymethyl cellulose (CMC), potassium persulfate (KPS), and ethanol were purchased from Merck, Germany. All the chemicals were used as received.

2.2. Preparation of the Ni-NPs

$NiCl_2{\cdot}6H_2O$, 80% N_2H_4 H_2O, and 50% NaOH aqueous solution were used as the source materials for the preparation of Ni-NPs. The reaction solution was prepared by dissolving $NiCl_2{\cdot}6H_2O$ in distilled water in a beaker. Under vigorous stirring, 80% N_2H_4 H_2O was added to the solution instantaneously, and the solution temperature was increased to 80 °C to form a Ni complex of $NiCl_2$ and N_2H_4. After complex formation, the 50 wt% NaOH solution was added, which turned the complex into a black precipitate of Ni-NPs. The black Ni precipitates were washed several times with distilled water and dried at room temperature.

2.3. Preparation of the Ni–CMC crosslinker

Ni-NPs were added to a mixture containing urea and a 50% NaOH solution. The resultant mixture was stirred for 15 min and kept in the refrigerator at −12 °C for 1 hour. After that,

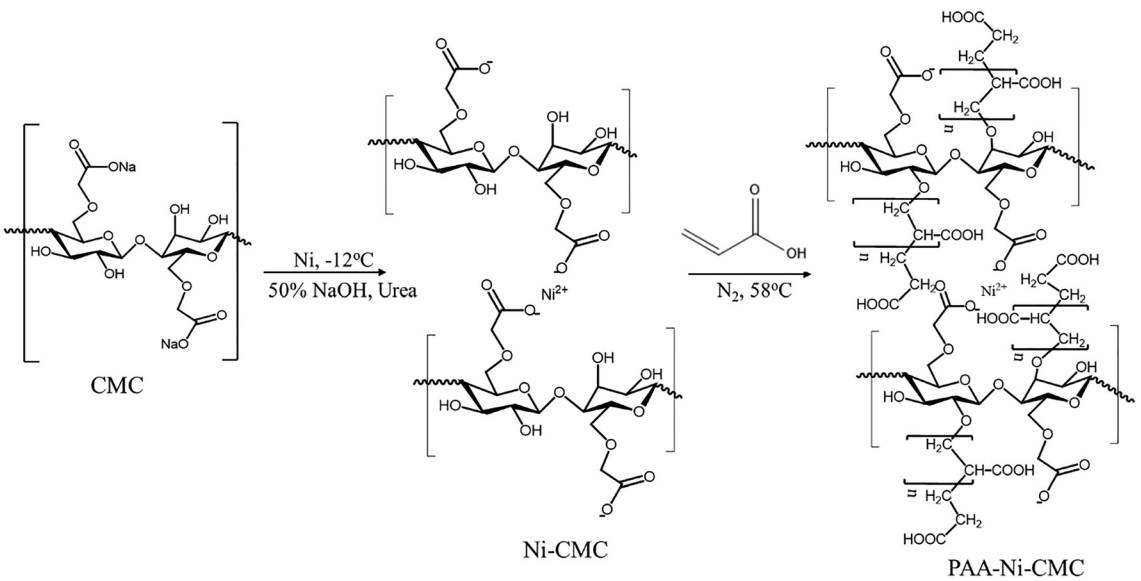

Fig. 1 Schematic of the PAA–Ni–CMC synthesis.

CMC was added, followed by stirring for 15 min and freezing at −12 °C for another 1 hour. The produced Ni–CMC crosslinker was then washed several times with distilled water and dried at room temperature.

2.4. Preparation of the PAA–Ni–CMC, PAA–CMC and PAA–Ni hydrogels

The cross-linked PAA composite hydrogels were synthesized using acrylic acid (AA) as the monomer, KPS as the initiator, and the prepared Ni–CMC as the crosslinker. 2 mL of the AA monomer was taken in a test tube, and a specified amount of Ni–CMC was added to it, followed by stirring for about 30 min. In another test tube, a specific weight of KPS was dissolved in 1 mL of DI water and sonicated for 30 min. The initiator was then transferred to the test tube containing the AA–Ni–CMC solution under vigorous stirring. After nitrogen gas bubbling, the mixture was poured into a glass mold consisting of two parallel glass plates separated by 2 mm silicone spacers. The sample was then heated at 56 °C for 8 hours to carry out the polymerization reaction. The schematic diagram for the synthesis of PAA–Ni–CMC hydrogel is shown in Fig. 1. In addition to the PAA–Ni–CMC composite hydrogel, PAA–Ni and PAA–CMC hydrogels were prepared using the same protocol for comparative analysis. After completing the polymerization, the prepared hydrogels were removed from the glass plates and stored for the characterization of the properties.

2.5. Characterization

The Fourier transform infrared (FTIR) spectra of Ni-NPs, carboxymethyl cellulose (CMC), and the nickel–CMC-based crosslinker (NCBC) were recorded in the 4000–400 cm^{-1} range using a Shimadzu FTIR-8400 instrument by preparing KBr pellets with samples. UV-vis absorption spectra were measured in a UV/visible spectrophotometer (Shimadzu-1800). Thermogravimetric analysis (TGA) and differential scanning calorimetry (DSC) were performed using a NETZSCH STA 449F3 instrument. The samples were heated at a temperature increase rate of 10 °C min^{-1} from room temperature to 1200 °C under a nitrogen atmosphere. The surface morphology of the prepared crosslinkers and hydrogels was studied using a field-emission scanning electron microscope (FESEM, JSM-7600F, Tokyo, Japan) at a voltage of 10.0 kV. The samples for FESEM were completely freeze-dried before performing the experiment. The magnetic properties of the samples were analysed with a vibrating sample magnetometer (VSM8604, Lake Shore Cryotronics). The conductivity of the samples was measured as a function of the frequency at room temperature using an impedance analyser.

3. Results and discussion

3.1. Characterization of Ni-NPs and the Ni–CMC crosslinker

The prepared Ni-NPs and Ni–CMC crosslinker were characterized by FTIR spectroscopy. The successful incorporation of the Ni-NPs was confirmed by comparing the FTIR spectrum of the Ni–CMC composite with the spectra of Ni-NPs and CMC, as shown in Fig. 2. The FTIR spectrum of Ni-NPs shows absorption bands at 3300 cm^{-1}, 1633 cm^{-1}, 1403 cm^{-1}, 1076 cm^{-1}, and 465 cm^{-1}, corresponding to the O–H stretching, stretching vibration of the CHO group, C–H bending, C–O stretching, and Ni–O stretching, respectively.[49] The wide band at about 3369 cm^{-1} is related to O–H stretching in pure CMC compounds. This broad band is transformed into a narrow band at 3334 cm^{-1} in the spectrum of the Ni–CMC crosslinker owing to the formation of a chemical bond on the interface of Ni-NPs.

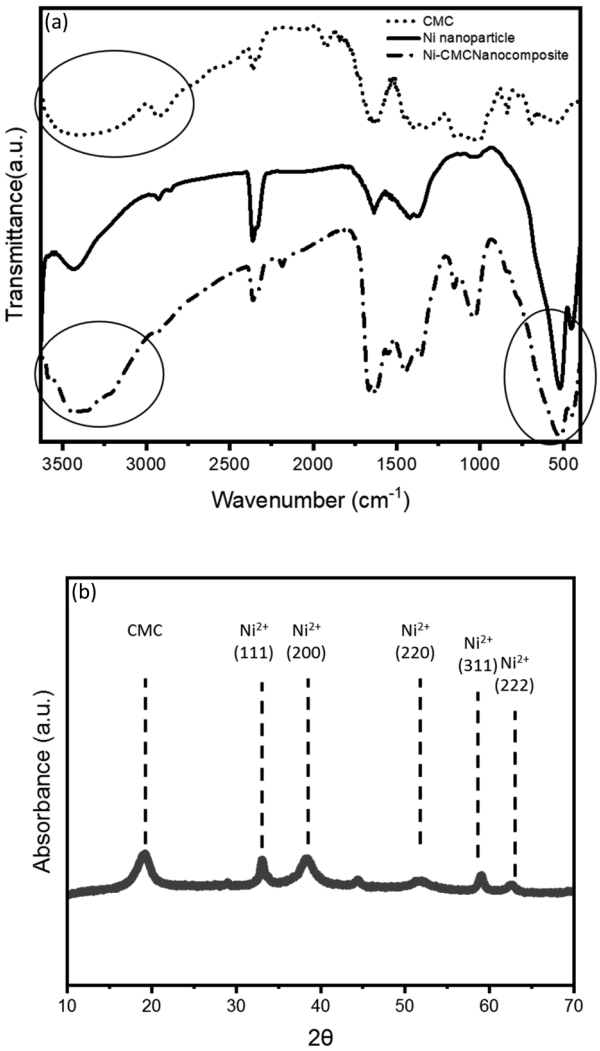

Fig. 2 (a) FTIR spectra of Ni-NPs, CMC, and the Ni–CMC crosslinker. (b) XRD spectrum of the Ni–CMC crosslinker.

Furthermore, the peaks at 2897, 1650, and 1033 cm^{-1} are attributed to C–H stretching, COO^- (asymmetric) stretching, and C–O symmetric stretching, respectively, for the Ni–CMC crosslinker, while these peaks are found at 2871, 1605, and 1006 cm^{-1}, respectively, for CMC. These findings suggest the presence of Ni-NPs among the free COO^- group in the ring of CMC. The lone pair on the O^- heteroatoms in CMC may be transferred to the unoccupied d-orbital of Ni-NPs to form coordination covalent bonds.

The peak of O–H is found to be comparatively broader in CMC, but it becomes a bit narrower in the Ni–CMC crosslinker.

In addition, the characteristic peak of the Ni–CMC crosslinker at 457 cm^{-1} has been assigned to Ni–O vibrations. The FTIR peaks observed for the Ni–CMC crosslinker are in agreement with the reported data.[50,51]

The XRD pattern of the Ni–CMC composite shows several well-defined diffraction peaks that confirm the successful incorporation of Ni^{2+} species within the CMC matrix. Distinct reflections appear at different positions, corresponding to characteristic lattice planes associated with Ni-containing domains. The presence of these peaks, alongside the broad amorphous background originating from the CMC polymer, indicates that Ni^{2+} ions interact strongly with the carboxylate groups of CMC, forming coordinated crosslinking sites rather than crystalline metallic Ni or higher-valence nickel oxides. Similar diffraction peaks have been reported for NiO–CMC composite beads.[52]

The successful incorporation of Ni-NPs in CMC was further confirmed by analysing and comparing the surface microstructure and morphology of Ni-NPs and the Ni–CMC crosslinker *via* field-emission scanning electron microscopy (FESEM), as shown in Fig. 3. The surface morphology shows that the average diameter of the Ni–CMC crosslinker is significantly larger than that of the Ni-NPs. This indicates that the CMC has been coated on the Ni-NP surface.

The EDS mapping of the Ni–CMC nanocomposite shows distinct peaks of Ni, C, and O, confirming successful composite formation. The characteristic Ni signals at ~0.85 keV and ~7.47 keV verify the presence of nickel nanoparticles, while the C Kα (~0.27 keV) and O Kα (~0.52 keV) peaks originate from the CMC coating. Elemental mapping reveals the uniform distribution of Ni, along with C and O, indicating the effective CMC coating and stabilization of Ni nanoparticles.

3.2. Thermal properties of CMC and the Ni–CMC crosslinker

The thermal properties of CMC and the Ni–CMC crosslinker were studied using TGA analysis. The TGA and DTGA plots are shown in Fig. 4. It is found that CMC loses about 81% its initial mass up to 1200 °C, and the Ni–CMC crosslinker loses only about 46% of its initial mass up to 1200 °C. This indicates the superior thermal stability of the Ni–CMC crosslinker compared with CMC. The DTGA curve indicates three major weight loss points for CMC. The first one is near 90 °C due to moisture removal, the second one is at about 200 °C due to CO_2 removal from the $-COO^-$ of CMC, and the third one is at approximately 300 °C due to C–O–C breakdown from CMC. On the other hand, the Ni–CMC crosslinker shows five major weight loss points. The first one is at about 90 °C due to moisture and H_2O removal; the second one is near 200 °C due to CO_2 removal from $-COO^-$; the third one is at about 250 °C, most probably due to the breakdown of electrostatic interactions between Ni^{2+} and $-COO^-$; the fourth one is at approximately 300 °C due to C–O–C breakdown; and the fifth one is at about 400 °C, most probably due to Ni–O coordination interaction breakdown.

CMC loses 12.39% of its mass at 200 °C due to CO_2 removal from the $-COO^-$ group, but Ni–CMC loses only 5.28% of its initial mass at 200 °C due to CO_2 removal from the $-COO^-$ group, which indicates that a large portion of COO^- is already involved in electrostatic interactions with Ni^{2+}. CMC loses 34.56% of its mass at 300 °C due to C–O–-C breakdown, but Ni–CMC loses only 13.75% of its initial mass at 300 °C due to C–O–C breakdown, which indicates that a large amount of O atoms of C–O–C is already involved in coordination bonding interactions with Ni^{2+}. All these data indicate the higher thermal stability of the Ni–CMC composite compared with CMC.

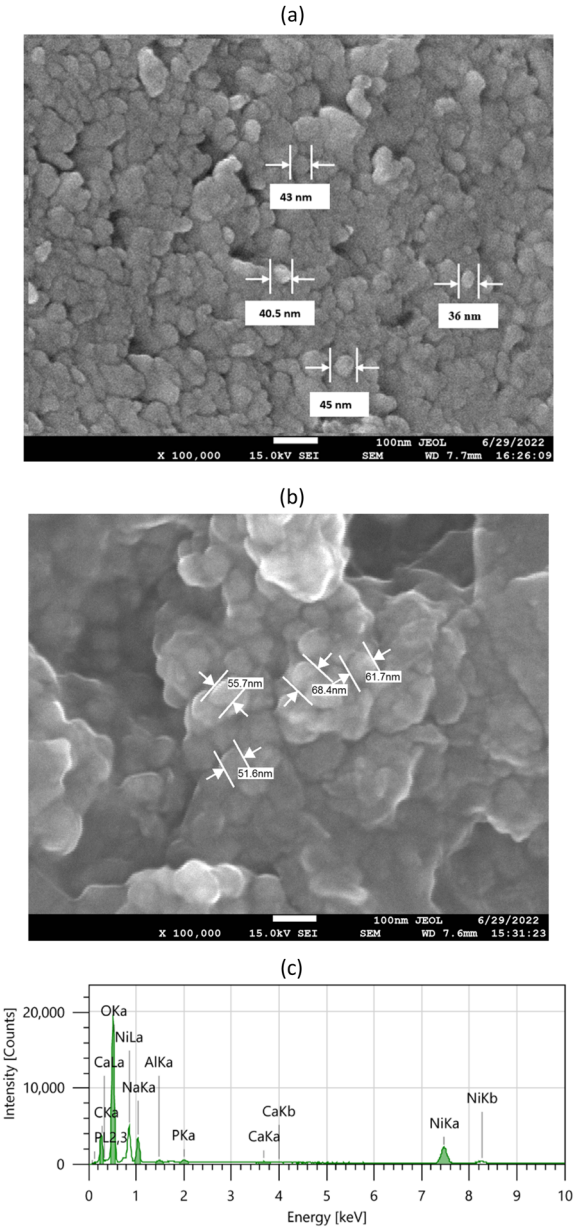

Fig. 3 FESEM images of (a) Ni-NPs and (b) Ni–CMC crosslinker. (c) EDS elemental mapping of the Ni–CMC crosslinker.

3.3. Mechanical properties of PAA–CMC, PAA–Ni and the PAA–Ni–CMC hydrogels

Tensile measurements were conducted in a systematic way to investigate the mechanical behavior of hydrogels and hydrogel nanocomposites. The tensile stress–strain curves of PAA–CMC,

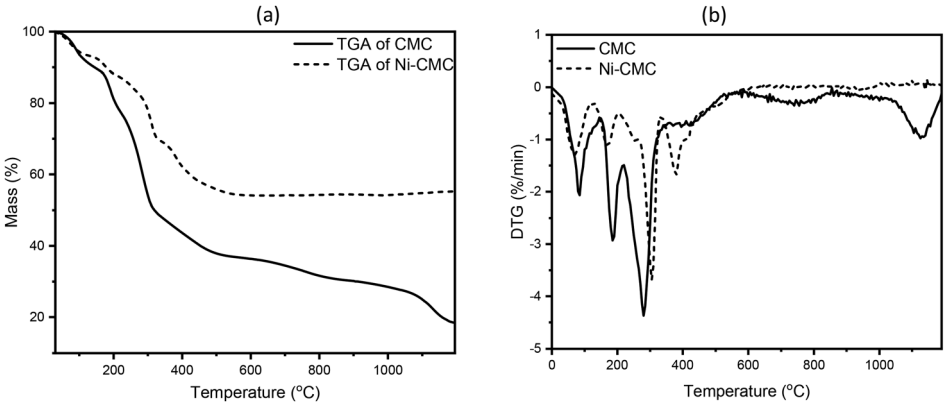

Fig. 4 (a) TGA curves of CMC and the Ni–CMC crosslinker. (b) DTG curves of CMC and the Ni–CMC crosslinker.

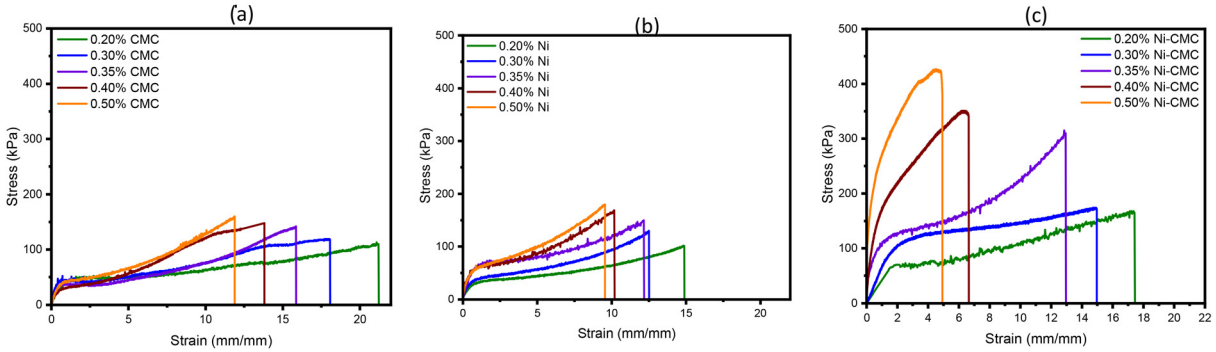

Fig. 5 Stress–strain curves of the (a) PAA–CMC, (b) PAA–Ni and (c) PAA–Ni–CMC hydrogels with different concentrations of crosslinkers.

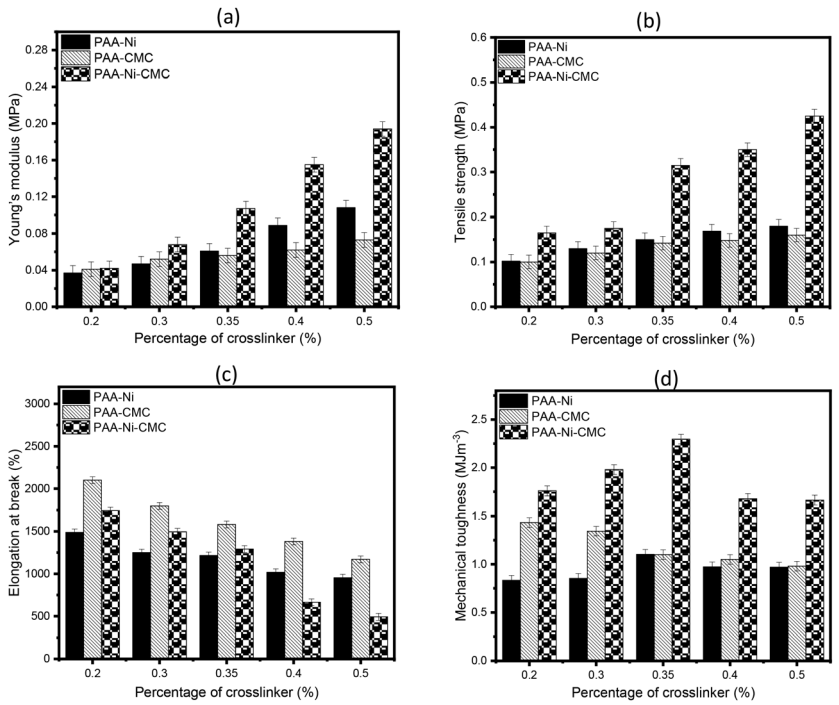

Fig. 6 Comparison of the (a) Young's modulus, (b) tensile strength, (c) elongation at break, and (d) mechanical toughness of PAA–Ni, PAA–CMC and PAA–Ni–CMC hydrogels with varying concentrations of the crosslinker.

Table 1 Comparison of the mechanical properties of various PAA hydrogels with reported values

Hydrogels	Young's modulus (kPa)	Tensile strength (kPa)	Elongation at break (%)	Toughness (kJ m^{-3})	Ref.
PAA–GO–Fe^{3+}	32	272	2185	3400	22
PAA–MBA	133	225	670	950	22
PAA–GOBC	161	248	4078	7124	22
PAA–CNC	27	142	1107	—	53
PAA–Si	30	157	987	1385	54
PAA–HB	247	188	513	—	55
PAA–GO	215	194	527	—	55
PAA–HB–GO	265	251	745	—	55
PAA–NCC	170	144	243	—	56
PAA–DANC	170	124	220	—	56
PAA–DCNC	297	209	786	—	56
PAA–Ni	108	180	1488	1104	This work
PAA–CMC	73	160	2100	1433	This work
PAA–Ni–CMC	194	425	1745	2297	This work

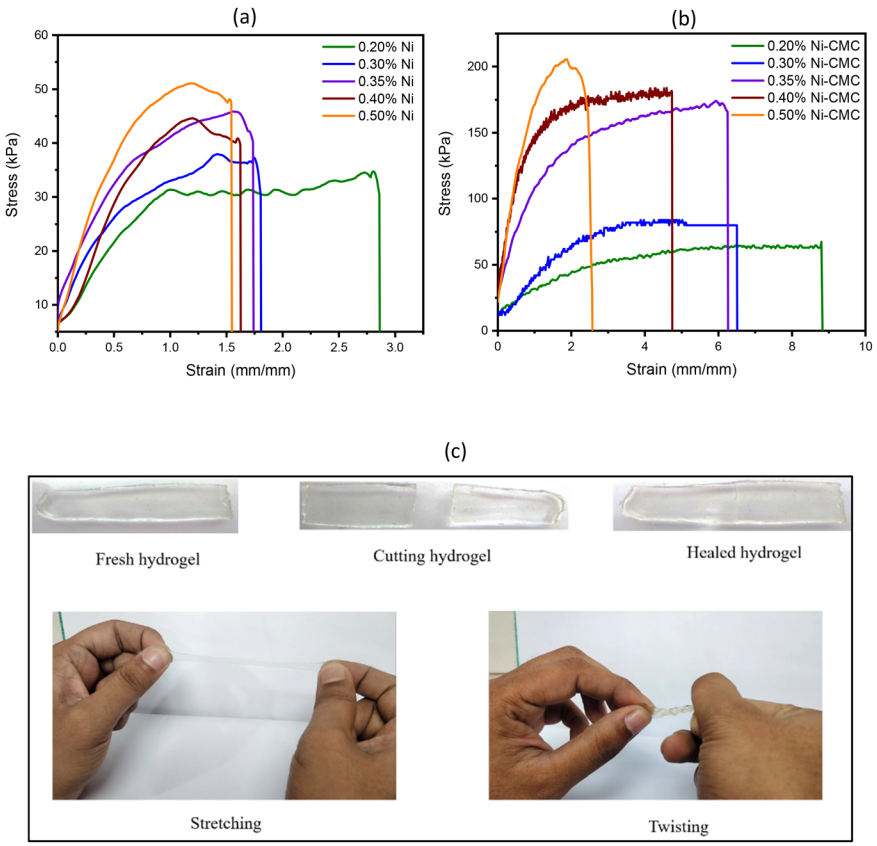

Fig. 7 Comparison of the self-healing efficiency of the (a) PAA–Ni, (b) PAA–Ni–CMC composite hydrogels and (c) the real time images demonstrating the self-healing efficiency.

PAA–Ni, and PAA–Ni–CMC hydrogels with different concentrations of Ni-NPs are compared in Fig. 5. The mechanical properties of these hydrogels have also been compared in a bar plot, as shown in Fig. 6. The mechanical toughness of the PAA–CMC hydrogel improves with increasing percentage of CMC in the PAA hydrogel. However, the toughness increases up to 0.35% Ni-NPs for the PAA–Ni hydrogel, and then, the toughness decreases with a further increase in the percentage of Ni-NPs. This increasing and decreasing pattern in the mechanical toughness has also been found when using Ni–CMC as the crosslinker in the PAA hydrogel. Though the PAA–Ni–CMC hydrogel exhibits much better mechanical toughness than the PAA–Ni hydrogel, in both cases, the mechanical toughness increases with increasing percentage of the crosslinker (up to 0.35%) and then decreases with a further increase in the crosslinker percentage.

The Young's modulus, tensile strength, and toughness of the hydrogels were evaluated from the stress–strain curves. The incorporation of Ni-NPs into the PAA hydrogels results in higher values of Young's modulus and tensile strength, which

increase when the amount of Ni-NPs is increased. When using Ni–CMC as a crosslinker in the PAA hydrogel, the increase in the Young's modulus and tensile strength is more prominent. However, the effect of the variation of CMC content in the mechanical properties of PAA hydrogels was found to be insignificant. The incorporation of a higher percentage of crosslinkers increases the bond density in the polymer network, which is responsible for the increase in Young's modulus and tensile strength. CMC, Ni-NPs, and Ni–CMC crosslinker-incorporated PAA hydrogels exhibit the same decreasing trend for the elongation at breaking. The incorporation of more crosslinkers increases the bond density in the polymer chain, which is responsible for making the hydrogel tougher and decreasing the elongation.

The mechanical properties of the PAA-based hydrogels containing different types of crosslinkers are listed in Table 1. It can be seen that the Ni–CMC crosslinker provides significantly better mechanical strength than most of the crosslinkers reported in recent studies on PAA-based hydrogels.

3.4. Self-healing properties

The self-healing properties of the PAA–Ni and PAA–Ni–CMC hydrogels having different percentages of crosslinkers were investigated. To do that, the prepared hydrogels were cut into two pieces. Then, the cut surfaces were kept in contact for a specific period at room temperature, after which the tensile tests were performed to assess the self-healing efficiency. The pieces merge over time due to their dynamic bond formation. It is found that after self-healing, the gels can be bent, twisted and stretched to a large extent without fracture, which demonstrates the excellent self-healing capacity of the prepared hydrogels.

The stress–strain curves of the PAA–Ni and PAA–Ni–CMC hydrogels with different concentrations of crosslinkers after self-healing and the real-time images demonstrating the self-healing ability of PAA–Ni–CMC hydrogels are shown in Fig. 7, and the corresponding recovery percentages of the tensile strength, elongation at break, and mechanical toughness of the same hydrogels are shown in Fig. 8. The real-time images clearly illustrate crack closure and reconnection at the damaged interface, providing direct visual evidence of the self-healing ability. The healed PAA–Ni–CMC hydrogels are also found to be strong enough to be stretched and twisted to a reasonable extent. Using a hybrid network constructed by a combination of reversible physical crosslinking, it is shown that it is possible to significantly enhance the mechanical characteristics of hydrogels while still retaining their self-healing capability.

As can be seen in Fig. 8, the recovery percentage for the hydrogels containing the Ni–CMC crosslinker is significantly higher than for those containing Ni-NP only. The better self-healing properties of PAA–Ni–CMC hydrogels can mainly be attributed to the reversible noncovalent bonds in the 3D networks (such as hydrogen bonds in the Ni–CMC and PAA network and coordination interactions in the PAA and Ni–CMC network). On the contrary, PAA–Ni hydrogels contain only ionic and coordination bonds, leading to a much lower recovery percentage compared with PAA–Ni–CMC hydrogels.

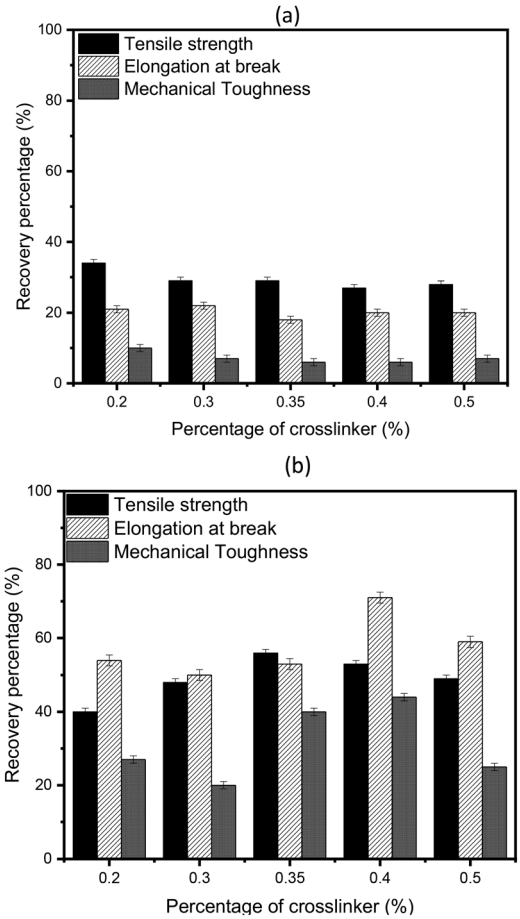

Fig. 8 Comparison of the self-recovery efficiency of the (a) PAA–Ni and (b) PAA–Ni–CMC composite hydrogels.

The PAA–Ni–CMC with 0.35% hydrogels recovers as much as about 56% of its tensile strength within 24 h. However, the maximum recovery in the elongation at break and mechanical toughness is observed for the PAA–Ni–CMC hydrogel with 0.4% crosslinker.

The self-healing performance of hydrogels mainly depends on the amount of ionic interactions formed between the Ni^{2+} ions and PAA chains. The ionic interactions are strong and reversible in nature. When the hydrogels are separated by cutting and the damaged regions are put in contact, the Ni^{2+} ions and COO^- groups of PAA are attracted to each other by ionic interactions and form coordination bonds, contributing to the healing of the fracture. In addition, the Ni–CMC provides coordination interactions and hydrogen bonding sites to regain the original mechanical performance. However, due to the lack of hydrogen bonds, PAA–Ni exhibits inferior self-healing. Adding Ni–CMC in the polymer matrix of PAA remarkably improves the self-healing performance due to the considerable coordination interactions between nickel ions and COO^- groups and hydrogen bonds provided by both PAA and the Ni–CMC crosslinker.

3.5. Conductivity of the PAA–Ni–CMC hydrogel

Electrical conductivity in the polymer hydrogels can be imparted either by using an electrically conductive monomer

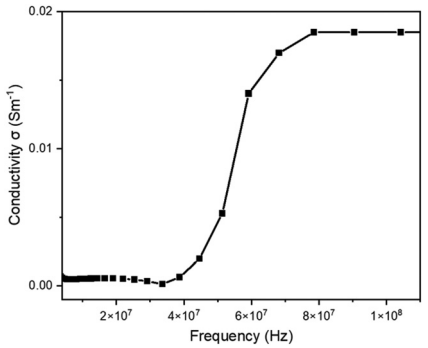

Fig. 9 Electrical conductivity of the PAA–Ni–CMC composite hydrogel.

Table 2 Comparison of the electrical conductivity of different types of conducting hydrogels

Nanoparticles	Hydrogels	Conductivity (S m^{-1})	Ref.
Au	Chitosan–gold nanoparticles	0.13	57
Au	Collagen–gold nanoparticles	1.3×10^{-6}	58
Ag	Collagen–silver nanoparticles	8×10^{-7}	58
Ag	Lignin–silver	2.9	59
Ag	Alginate–silver	0.001–100	60
W	Alginate–tungsten	0.0001–100	60
Fe	Fe_3O_4–MoS_2–PANI	0.2	61
Cu	Polyacrylamide–Cu	0.001	62
Ni	Polyacrylic acid–Ni–cellulose	1.9	This work

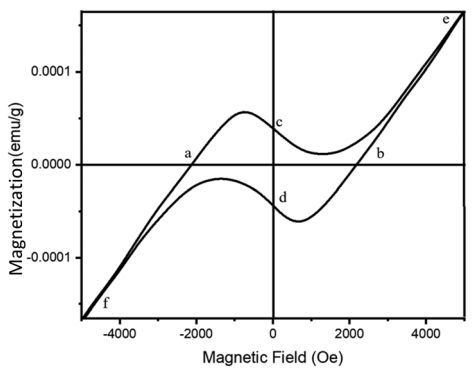

Fig. 10 Magnetic hysteresis loop of the PAA–Ni–CMC composite hydrogel showing the coercivity (a), retentivity (c), and maximum saturation point (e).

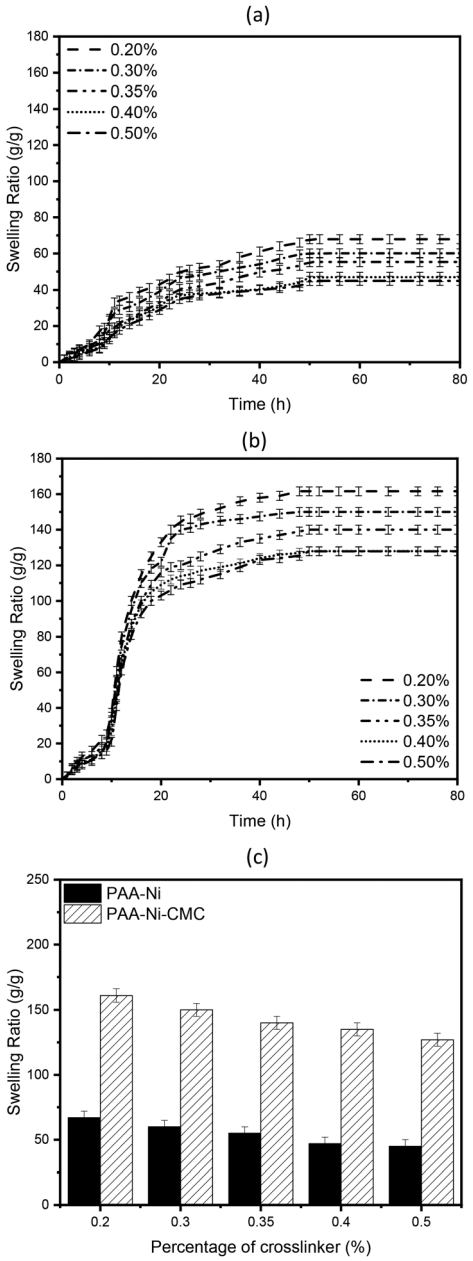

Fig. 11 Swelling behaviour of the as-prepared (a) PAA–Ni hydrogels and (b) PAA–Ni–CMC hydrogels with different concentrations of crosslinkers, (c) comparison of swelling ratios of PAA–Ni and PAA–Ni–CMC hydrogels.

or by doping with other electrically conductive materials. In this study, as Ni-NPs have been incorporated in the hydrogel network as the crosslinker, which are one of the well-known conductive metals, it is expected that the PAA–Ni–CMC hydrogel materials will be electrically conductive. The conductivity of the PAA–Ni–CMC hydrogel nanocomposite was recorded as a function of the frequency at room temperature using an impedance analyser, as shown in Fig. 9. The PAA–Ni–CMC composite hydrogel with 0.35% crosslinker shows an AC conductivity of about 1.9 S m^{-1}.

The electrical conductivity of a few other metal–hydrogels is summarized in Table 2. It is found that the conductivity of PAA–Ni–CMC composite hydrogels is comparable with the conductivity reported for other similar types of metal-hydrogel nanocomposites.

3.6. Magnetic properties of the PAA–Ni–CMC composite hydrogel

The magnetic property of the PAA–Ni–CMC composite hydrogel was measured using a vibrating sample magnetometer (VSM). The magnetic hysteresis loop for the PAA–Ni–CMC with 0.35% Ni–CMC crosslinker is shown in Fig. 10, showing the coercivity, retentivity, and maximum saturation point. The maximum

saturation magnetization of the PAA–Ni–CMC nanocomposite was found to be 0.00017 emu per g. The prepared hydrogel nanocomposite also exhibited moderate retentivity (0.00004 emu per g) and coercivity (2062 Oe), as shown in the hysteresis loop.

3.7. Swelling properties of PAA–Ni and the PAA–Ni–CMC composite hydrogels

The crosslinking ability of Ni and Ni–CMC crosslinkers in PAA–Ni and PAA–Ni–CMC hydrogels, respectively, was investigated by studying the swelling behaviour. The swelling kinetics of the PAA nanocomposite hydrogels with different concentrations of the crosslinker are shown in Fig. 11.

The nature of crosslinking and the crosslinking density of the hydrogel network play important roles in the swelling ratio. It was observed that the PAA hydrogel with Ni-NPs absorbed a large amount of water over time. The swelling capacity increased significantly after 48 h. The PAA hydrogels with Ni-NPs showed less swelling kinetics. However, when the Ni–CMC crosslinker was incorporated into the PAA composite hydrogels, the swelling capacity was found to increase, and the swelling ratio was stable after 48 h. The addition of the Ni–CMC crosslinker increased the swelling capacity of the PAA hydrogel. CMC has a great water retention capacity, which is responsible for the increased swelling behaviour of all PAA–Ni–CMC hydrogels.

4. Conclusions

We successfully developed the Ni–CMC crosslinker, in which Ni-NPs improve the mechanical toughness of the hydrogel and impart magnetism into the prepared composite hydrogel. The incorporation of Ni-NPs into CMC was confirmed using FESEM by comparing the nanoparticle size, and FTIR also showed the characteristic peaks of the Ni–CMC crosslinker. The PAA–Ni–CMC composite hydrogel was prepared using free radical polymerization, with KPS as the initiator. The mechanical toughness and self-healing capability of the hydrogel were studied by varying the composition of Ni-NPs in the hydrogel. It was found that the hydrogel with a lower percentage of Ni-NPs showed better elongation at break than the hydrogel with a higher percentage of Ni-NPs. As the percentage of Ni-NPs increased, the elongation at break of the hydrogel decreased, while its tensile strength increased. The prepared hydrogel also showed significant self-healing capability due to the physical bonding sites offered by the CMC network. The PAA–Ni–CMC hydrogel showed almost 60% recovery in tensile strength, while the recovery in elongation at break was more than 70%. Most importantly, the prepared hydrogel showed responsiveness to a magnetic field, as characterized by a Gauss meter. This responsive nature of the hydrogel and excellent mechanical toughness and self-healing capability highlights the strong potential of PAA–Ni–CMC composite hydrogel advanced applications, particularly in soft robotics, biosensors and controlled drug delivery.

Author contributions

Md. Sohanur Rahman: conceptualization; formal analysis; investigation; methodology; figure drawing; and writing – original draft. Maisha Rahman: investigation (supporting) and writing – review and editing (supporting). Md. Mahamudul Hasan Rumon: conceptualization (supporting); investigation (supporting); and methodology (supporting). Chanchal Kumar Roy: investigation (supporting) and methodology (supporting). Md. Mahbub Alam: conceptualization; formal analysis; investigation; methodology; resources; supervision; project administration; and writing – review and editing.

Conflicts of interest

There are no conflicts to declare.

Data availability

All data supporting the findings of this study are included within the manuscript. Additional raw data are available from the corresponding author, Dr Md. Mahbub Alam, upon reasonable request.

Acknowledgements

The study was conducted using the instrumental support of the Bangladesh University of Engineering and Technology (BUET) which was purchased under different projects approved by the Committee for Advanced Studies and Research (CASR), BUET.

References

1 H. M. El-Husseiny, E. A. Mady, W. A. El-Dakroury, A. S. Doghish and R. Tanaka, Stimuli-responsive hydrogels: smart state of-the-art platforms for cardiac tissue engineering, *Front. Bioeng. Biotechnol.*, 2023, **11**, 1174075.
2 Y. Wang, J. Li, M. Tang, C. Peng, G. Wang, J. Wang, X. Wang, X. Chang, J. Guo and S. Gui, Smart stimuli-responsive hydrogels for drug delivery in periodontitis treatment, *Biomed. Pharmacother.*, 2023, **162**, 114688.
3 X. Sun, S. Agate, K. S. Salem, L. Lucia and L. Pal, Hydrogel-Based Sensor Networks: Compositions, Properties, and Applications-A Review, *ACS Appl. Bio Mater.*, 2021, **4**(1), 140–162.
4 A. S. Hoffman, Hydrogels for biomedical applications, *Adv. Drug Delivery Rev.*, 2012, **64**, 18–23.
5 M. K. Yazdi, V. Vatanpour, A. Taghizadeh, M. Taghizadeh, M. R. Ganjali, M. T. Munir, S. Habibzadeh, M. R. Saeb and M. Ghaedi, Hydrogel membranes: a review, *Mater. Sci. Eng., C*, 2020, **114**, 1–20.
6 F. Hapiot, S. Menuel and E. Monflier, Thermoresponsive Hydrogels in Catalysis, *ACS Catal.*, 2013, **3**(5), 1006–1010.
7 J. L. Drury and D. J. Mooney, Hydrogels for tissue engineering: scaffold design variables and applications, *Biomaterials*, 2003, **24**(24), 4337–4351.

8 Z. Jiang, M. L. Tan, M. Taheri, Q. Yan, T. Tsuzuki and M. G. Gardiner, Strong, Self-Healable, and Recyclable Visible-Light-Responsive Hydrogel Actuators, *Angew. Chem.*, 2020, **59**(18), 7049–7056.

9 O. Werzer, S. Tumphart, R. Keimel, P. Christian and A. M. Coclite, Drug release from thin films encapsulated by a temperature-responsive hydrogel, *Soft Matter*, 2019, **15**(8), 1853–1859.

10 M. Ding, L. Jing, H. Yang, C. E. Machnicki, X. Fu, K. Li, I. Y. Wong and P. Y. Chen, Corrigendum to ''Multifunctional soft machines based on stimuli-responsive hydrogels: from freestanding hydrogels to smart integrated systems'' [Mater Today Adv 8 (2020) 100088], *Mater. Today Adv.*, 2021, **9**, 100130.

11 S. Liang, Q. M. Yu, H. Yin, Z. L. Wu, T. Kurokawa and J. P. Gong, Ultrathin tough double network hydrogels showing adjustable muscle-like isometric force generation triggered by solvent, *Chem. Commun.*, 2009, (48), 7518–7520.

12 A. Bhat, J. M. Amanor-Boadu and A. Guiseppi-Elie, Toward Impedimetric Measurement of Acidosis with a pH-Responsive Hydrogel Sensor, *ACS Sensors*, 2020, **5**(2), 500–509.

13 S. Mallawarachchi, V. Gejji, L. S. Sierra, H. Wang and S. Fernando, Electrical Field Reversibly Modulates Enzyme Kinetics of Hexokinase Entrapped in an Electro-Responsive Hydrogel, *ACS Appl. Bio Mater.*, 2019, **2**(12), 5676–5686.

14 W. Shi, J. Huang, R. Fang and M. Liu, Imparting Functionality to the Hydrogel by Magnetic-Field-Induced Nanoassembly and Macro-response, *ACS Appl. Mater. Interfaces*, 2020, **12**(5), 5177–5194.

15 H. Chavda and C. Patel, Effect of crosslinker concentration on characteristics of superporous hydrogel, *Int. J. Pharm. Invest.*, 2011, **1**(1), 17–21.

16 D. Ray, D. K. Mohapatra, R. K. Mohapatra, G. P. Mohanta and P. K. Sahoo, Synthesis and colon-specific drug delivery of a poly(acrylic acid-*co*-acrylamide)/MBA nanosized hydrogel, *J. Biomater. Sci., Polym. Ed.*, 2008, **19**(11), 1487–1502.

17 D. Zhao, J. Huang, Y. Zhong, K. Li, L. Zhang and J. Cai, High-Strength and High-Toughness Double-Cross-Linked Cellulose Hydrogels: A New Strategy Using Sequential Chemical and Physical Cross-Linking, *Adv. Funct. Mater.*, 2016, **26**(34), 6279–6287.

18 H. Espinosa-Andrews, C. Velásquez-Ordoñez, J. M. Cervantes-Uc and R. Rodríguez-Rodríguez, Water behavior, thermal, structural, and viscoelastic properties of physically cross-linked chitosan hydrogels produced by $NaHCO_3$ as a crosslinking agent, *J. Mater. Sci.*, 2023, **58**(13), 6025–6037.

19 M. M. H. Rumon, M. S. Rahman, A. A. Akib, M. S. Sohag, M. R. A. Rakib, M. A. R. Khan, F. Yesmin, M. S. Shakil and M. M. Rahman Khan, Progress in hydrogel toughening: addressing structural and crosslinking challenges for biomedical applications, *Discovery Mater.*, 2025, **5**(1), 5.

20 P. A. Song, Z. Xu, Y. Lu and Q. Guo, Bioinspired strategy for tuning thermal stability of PVA via hydrogen-bond crosslink, *Compos. Sci. Technol.*, 2015, **118**, 16–22.

21 D. Hu, M. Zeng, Y. Sun, J. Yuan and Y. Wei, Cellulose-based hydrogels regulated by supramolecular chemistry, *SusMat*, 2021, **1**(2), 266–284.

22 S. D. Sarkar, M. M. Uddin, C. K. Roy, M. J. Hossen, M. I. Sujan and M. S. Azam, Mechanically tough and highly stretchable poly(acrylic acid) hydrogel cross-linked by 2D graphene oxide, *RSC Adv.*, 2020, **10**(18), 10949–10958.

23 M. Hafezi, S. N. Khorasani, S. Khalili and R. E. Neisiany, Self-healing interpenetrating network hydrogel based on GelMA/alginate/nano-clay, *Int. J. Biol. Macromol.*, 2023, **242**(Pt 2), 124962.

24 X. Sun, Z. Qin, L. Ye, H. Zhang, Q. Yu, X. Wu, J. Li and F. Yao, Carbon nanotubes reinforced hydrogel as flexible strain sensor with high stretchability and mechanically toughness, *Chem. Eng. J.*, 2020, **382**, 122832.

25 M. R. Karim, M. Harun-Ur-Rashid and A. B. Imran, Effect of sizes of vinyl modified narrow-dispersed silica cross-linker on the mechanical properties of acrylamide based hydrogel, *Sci. Rep.*, 2023, **13**(1), 5089.

26 Md Sohanur Rahman, *Enhancement of mechanical property of polyacrylic acid hydrogel using magnetic nanocomposite based crosslinker*, MSc thesis, Bangladesh University of Engineering and Technology, 2023.

27 H. Yuk, B. Lu and X. Zhao, Hydrogel bioelectronics, *Chem. Soc. Rev.*, 2019, **48**(6), 1642–1667.

28 H. Yuk, J. Wu and X. Zhao, Hydrogel interfaces for merging humans and machines, *Nat. Rev. Mater.*, 2022, **7**(12), 935–952.

29 X. Huang, C. Chen, X. Ma, T. Zhu, W. Ma, Q. Jin, R. Du, Y. Cai, M. Zhang and D. Kong, In situ forming dual-conductive hydrogels enable conformal, self-adhesive and antibacterial epidermal electrodes, *Adv. Funct. Mater.*, 2023, **33**(38), 2302846.

30 L. Inzelberg and Y. Hanein, Electrophysiology meets printed electronics: The beginning of a beautiful friendship, *Front. Neurosci.*, 2019, **12**, 992.

31 L. V. Kayser and D. J. Lipomi, Stretchable conductive polymers and composites based on PEDOT and PEDOT:PSS, *Adv. Mater.*, 2019, **31**(10), 1806133.

32 Y. Shi, C. Ma, L. Peng and G. Yu, Conductive ''smart'' hybrid hydrogels with PNIPAM and nanostructured conductive polymers, *Adv. Funct. Mater.*, 2015, **25**(8), 1219–1225.

33 N. K. Guimard, N. Gomez and C. E. Schmidt, Conducting polymers in biomedical engineering, *Prog. Polym. Sci.*, 2007, **32**(8–9), 876–921.

34 D. Mawad, A. Lauto and G. Wallace, *Polymeric Hydrogels as Smart Biomaterials*, 2016, ch. 2, DOI, 10, pp. 978–973.

35 C. Lim, Y. Shin, J. Jung, J. H. Kim, S. Lee and D.-H. Kim, Stretchable conductive nanocomposite based on alginate hydrogel and silver nanowires for wearable electronics, *APL Mater.*, 2019, **7**(3), 031502.

36 H. Wu, G. Yu, L. Pan, N. Liu, M. T. McDowell, Z. Bao and Y. Cui, Stable Li-ion battery anodes by in-situ polymerization of conducting hydrogel to conformally coat silicon nanoparticles, *Nat. Commun.*, 2013, **4**(1), 1943.

37 X. Zhao, X. Ding, Z. Deng, Z. Zheng, Y. Peng, C. Tian and X. Long, A kind of smart gold nanoparticle–hydrogel

composite with tunable thermo-switchable electrical properties, *New J. Chem.*, 2006, **30**(6), 915–920.

38 N. Amreddy, A. Babu, R. Muralidharan, J. Panneerselvam, A. Srivastava, R. Ahmed, M. Mehta, A. Munshi and R. Ramesh, Recent Advances in Nanoparticle-Based Cancer Drug and Gene Delivery, *Adv. Cancer Res.*, 2018, **137**, 115–170.

39 J. Zhuang, R. H. Fang and L. Zhang, Preparation of particulate polymeric therapeutics for medical applications, *Small Methods*, 2017, **1**(9), 1700147.

40 Z. Chen, Small-molecule delivery by nanoparticles for anticancer therapy, *Trends Mol. Med.*, 2010, **16**(12), 594–602.

41 A. Sultana, M. Zare, V. Thomas, T. S. S. Kumar and S. Ramakrishna, Nano-based drug delivery systems: Conventional drug delivery routes, recent developments and future prospects, *Med. Drug Discovery*, 2022, **15**, 100134.

42 O. C. Farokhzad and R. Langer, Nanomedicine: Developing smarter therapeutic and diagnostic modalities, *Adv. Drug Delivery Rev.*, 2006, **58**(14), 1456–1459.

43 A. Z. Wang, R. Langer and O. C. Farokhzad, Nanoparticle delivery of cancer drugs, *Annu. Rev. Med.*, 2012, **63**, 185–198.

44 B. Malik Anjelh, T. Ahmad, Sunaryono, Munaji, S. Dita Puspita, D. Yanurita and Darminto, Development of PVA/Fe_3O_4 as Smart Magnetic Hydrogels for Biomedical Applications, in *Hydrogels*, ed. H. Sajjad and H. Adnan, IntechOpen, 2017, p. 8.

45 T.-Y. Liu, S.-H. Hu, K.-H. Liu, D.-M. Liu and S.-Y. Chen, Study on controlled drug permeation of magnetic-sensitive ferrogels: Effect of Fe_3O_4 and PVA, *J. Controlled Release*, 2008, **126**(3), 228–236.

46 A. Fernández-Ferreiro, M. González Barcia, M. Gil-Martínez, A. Vieites-Prado, I. Lema, B. Argibay, J. Blanco Méndez, M. J. Lamas and F. J. Otero-Espinar, In vitro and in vivo ocular safety and eye surface permanence determination by direct and Magnetic Resonance Imaging of ion-sensitive hydrogels based on gellan gum and kappa-carrageenan, *Eur. J. Pharm. Biopharm.*, 2015, **94**, 342–351.

47 M. Häring, J. Schiller, J. Mayr, S. Grijalvo, R. Eritja and D. D. Díaz, Magnetic Gel Composites for Hyperthermia Cancer Therapy, *Gels*, 2015, **1**(2), 135–161.

48 G. R. Mahdavinia, A. Afzali, H. Etemadi and H. Hoseinzadeh, Magnetic/pH-sensitive nanocomposite hydrogel based carboxymethyl cellulose –g- polyacrylamide/montmorillonite for colon targeted drug delivery, *Book Magnetic/pH-sensitive nanocomposite hydrogel based carboxymethyl cellulose – g-polyacrylamide/montmorillonite for colon targeted drug delivery*, 2017.

49 D. Yadav, A. K. Dixit, S. Raghothama and S. K. Awasthi, Ni nanoparticle-confined covalent organic polymer directed diaryl-selenides synthesis, *Dalton Trans.*, 2020, **49**(35), 12266–12272.

50 H. M. A. El-Lateef, W. A. Albokheet and M. Gouda, Carboxymethyl cellulose/metal (Fe, Cu and Ni) nanocomposites as non-precious inhibitors of C-steel corrosion in HCl solutions: synthesis, characterization, electrochemical and surface morphology studies, *Cellulose*, 2020, **27**(14), 8039–8057.

51 M. Nurguzhin, M. Janikeyev, M. Omarbayev, A. Yermakhanova, M. Meiirbekov, M. Zhumakhanov, A. Lesbayev, D. Yerezhep, M. Atamanov, M. Tulepov and Z. Beksultan, Optimizing Combustion Characteristics of Ammonium Perchlorate Composites with Nickel-Enhanced Carboxymethyl Cellulose, *Aerospace*, 2025, **12**(4), 270.

52 F. Ahmed, T. Gulzar, S. Kiran, I. Ahmad, A. Fatima, S. Yasir, W. F. Alhajaim, A. Khalil, M. Ul-Islam, E. M. Bakhsh and T. Kamal, Nickel oxide and carboxymethyl cellulose composite beads as catalyst for the pollutant degradation, *Appl. Nanosci.*, 2022, **12**(11), 3585–3595.

53 J. Yang, C.-R. Han, J.-F. Duan, M.-G. Ma, X.-M. Zhang, F. Xu, R.-C. Sun and X.-M. Xie, Studies on the properties and formation mechanism of flexible nanocomposite hydrogels from cellulose nanocrystals and poly(acrylic acid), *J. Mater. Chem.*, 2012, **22**(42), 22467–22480.

54 M. I. Sujan, S. D. Sarkar, S. Sultana, L. Bushra, R. Tareq, C. K. Roy and M. S. Azam, Bi-functional silica nanoparticles for simultaneous enhancement of mechanical strength and swelling capacity of hydrogels, *RSC Adv.*, 2020, **10**(11), 6213–6222.

55 Y. Yu, L. C. X. De Andrade, L. Fang, J. Ma, W. Zhang and Y. Tang, Graphene oxide and hyperbranched polymer-toughened hydrogels with improved absorption properties and durability, *J. Mater. Sci.*, 2015, **50**(9), 3457–3466.

56 M. A. Hossain, C. K. Roy, S. D. Sarkar, H. Roy, A. H. Howlader and S. H. Firoz, Improvement of the strength of poly(acrylic acid) hydrogels by the incorporation of functionally modified nanocrystalline Cellulose, *Mater. Adv.*, 2020, **1**(6), 2107–2116.

57 P. Baei, S. Jalili-Firoozinezhad, S. Rajabi-Zeleti, M. Tafazzoli-Shadpour, H. Baharvand and N. Aghdami, Electrically conductive gold nanoparticle-chitosan thermosensitive hydrogels for cardiac tissue engineering, *Mater. Sci. Eng., C*, 2016, **63**, 131–141.

58 G. Kougkolos, M. Golzio, L. Laudebat, Z. Valdez-Nava and E. Flahaut, Hydrogels with electrically conductive nanomaterials for biomedical applications, *J. Mater. Chem. B*, 2023, **11**(10), 2036–2062.

59 J. Cai, X. Zhang, W. Liu, J. Huang and X. Qiu, Synthesis of highly conductive hydrogel with high strength and super toughness, *Polymer*, 2020, **202**, 122643.

60 C. M. Tringides, M. Boulingre and D. J. Mooney, Metal-based porous hydrogels for highly conductive biomaterial scaffolds, *Oxford Open Mater. Sci.*, 2024, **3**(1), itad002.

61 H. Hu, X. Zhong, S. Yang and H. Fu, Tough and stretchable Fe_3O_4/MoS_2/PAni composite hydrogels with conductive and magnetic properties, *Composites, Part B*, 2020, **182**, 107623.

62 J. Lin, Q. Tang and J. Wu, The synthesis and electrical conductivity of a polyacrylamide/Cu conducting hydrogel, *React. Funct. Polym.*, 2007, **67**(6), 489–494.